Electronic Supplementary Material (ESI) for Soft Matter.

Microdynamics and arrest of coarsening during spinodal decomposition in thermoreversible colloidal gels

Yongxiang Gao[ab], Juntae Kim[a] and Matthew E. Helgeson[*a]

[a]*Department of Chemical Engineering, University of California Santa Barbara, Santa Barbara CA 93106*

[b]*Current address: Department of Chemistry, Physical and Theoretical Chemistry Laboratory, University of Oxford, South Parks Road, Oxford, OX1 3QZ, UK*

Electronic Supplementary Information

S1. Review of previous measurements on arrested colloidal gels

In Fig. S1, we have reviewed experimental results on microscopic dynamics of colloidal gels. Most of the previous studies have focused on length scales close to that of an individual particle. An emerging feature of colloidal gels from these studies is a short-time nearly arrested dynamics and a long-time hyperdiffusive dynamics, separated by a time scale on the order of 10^4-10^5 τ_B.

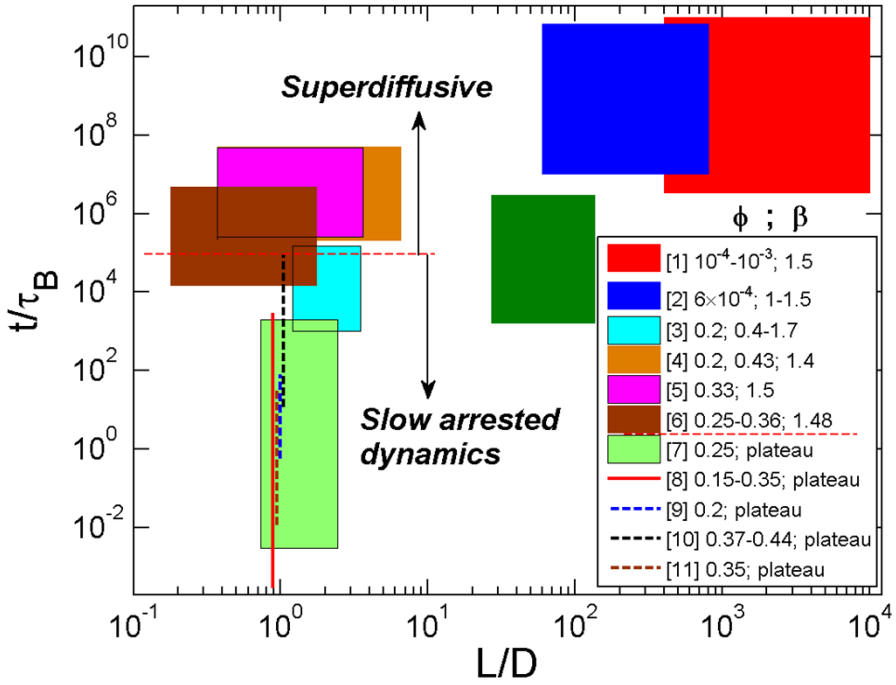

FIG. S1. Time and length scales of colloidal gels being explored in the literature, normalized by the Brownian time scale (τ_B), the time it takes for a free particle to diffuse a distance of its own radius, and diameter (D) of colloidal particles, respectively. Dark green patch represents the ranges investigated in this work. Dashed red line indicates an estimated critical time scale below which slow arrested dynamics or diffusive dynamics is observed and above which superdiffusive behavior is reported. Legend indicates both the volume fraction(s) studied; and the compressed exponent observed for the slow dynamics. "Plateau" indicates the observation of a long-time plateau in the correlation function.

S2. Interpolation of temperature-dependent interdroplet attractions

Fig. S2 below summarizes the data shown in Table S2 of ref. 42, where temperature-dependent SANS data on a dilute suspension of nanodroplets in the presence of PEGDA were fit to a structure factor corresponding to square well attractions with a well range of $\lambda/\sigma = 0.47$ and variable well depth ε. The data were fit to the following empirical sigmoidal relation,

$$\varepsilon(T)/k_bT = \frac{a}{1 + be^{-cT}} \tag{S1}$$

where a, b and c are adjustable parameters.

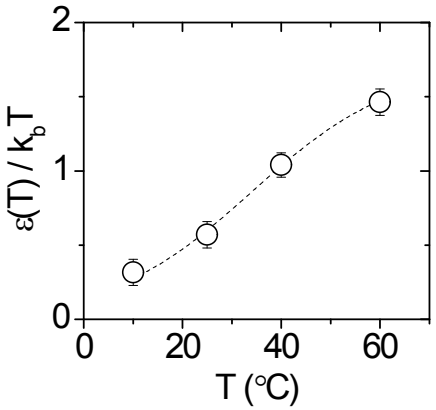

Fig. S2. Temperature-dependent well depth for a suspension of nanodroplets with $\phi = 0.01$ in an aqueous suspension containing 33 vol% PEGDA. Points correspond to best-fits from SANS data. Dashed line represents the best-fit of the data to equation S1, with the parameters a = 1.72±0.31, b = 10.4±4.3 and c = 0.069±0.021.

S3. Time-dependent rheology of various volume fractions and temperature quenches

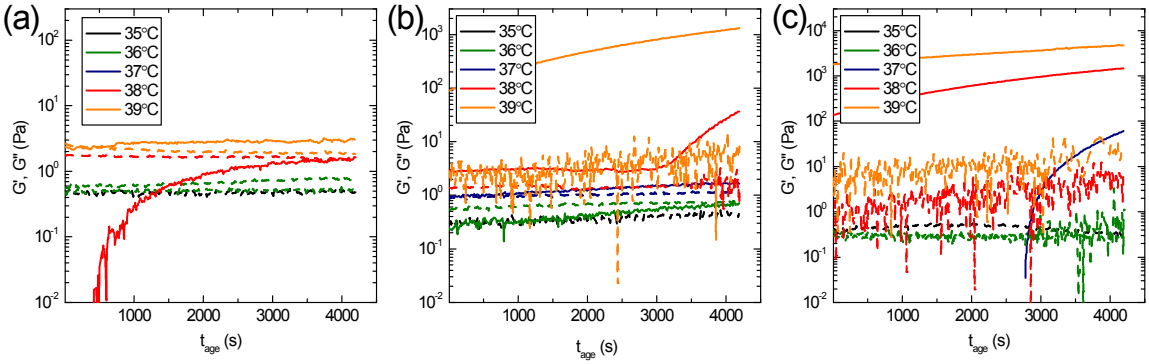

FIG. S3.1 Time-dependent elastic moduli (solid line) and viscous moduli (dashed line) of nanoemulsions at various temperatures (°C). (a) ϕ=0.27, (b) ϕ=0.20 and (c) ϕ=0.15. All samples contain 33 vol% PEGDA in the continuous phase, and were quickly quenched from room temperature to the temperatures indicated.

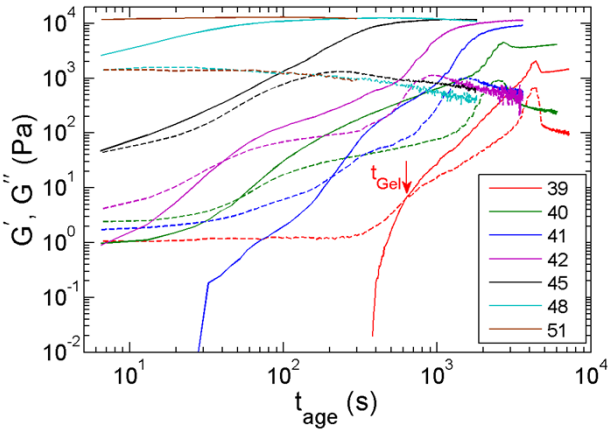

FIG. S3.2 Time-dependent elastic moduli (solid line) and viscous moduli (dashed line) of nanoemulsions at various temperatures (°C). Samples all contain ϕ=0.33 and 33 vol% PEGDA in the continuous phase, and were quickly quenched from room temperature to the temperatures indicated. The time (t_{Gel}) took by the sample to form a gel (defined by G'=G'') at 39°C, the temperature we perform the microscopy experiment, is indicated by an arrow.

S4. Potential effect of TAM in determining the characteristic domain size, L_c

Figure S4 compares two scalings – one where the raw FFT curves are scaled by the values of I_{max} and q_{max} from the raw image [inset of (a)], and one where they are rescaled by the values of I_{max} from the raw image and q_{max} obtained using TAM [inset of (b)]. Clearly, the inability to resolve a peak in the raw FFT produces very poor results when shifting, as judged by the fact that the high-q structure does not collapse. However, when the TAM values are used, reasonable collapse of the data is obtained. This further supports the fact that the peak in the TAM FFT is not an artifact.

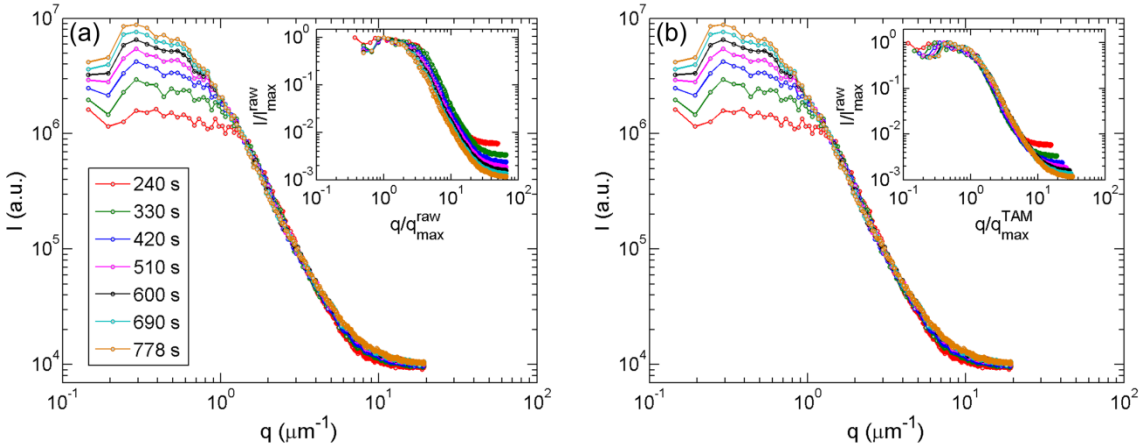

FIG. S4. Power spectra of raw optical images taking at T=39°C, which exhibit no clear peaks. Inset of (a): raw FFT curves are rescaled by the values of I_{max} and q_{max} from the raw images. Inset of (b): raw FFT curves are rescaled by the values of I_{max} from the raw images and q_{max} obtained using TAM.

Table S1: Optimized TAM parameters used in Figure 3a

t (s)	240	420	600	778
w (pixels)	11	14	20	22
wg (Pixels)	7	8	11	13

S5. Probing intensity fluctuation or structural reorganization within domains by DDM

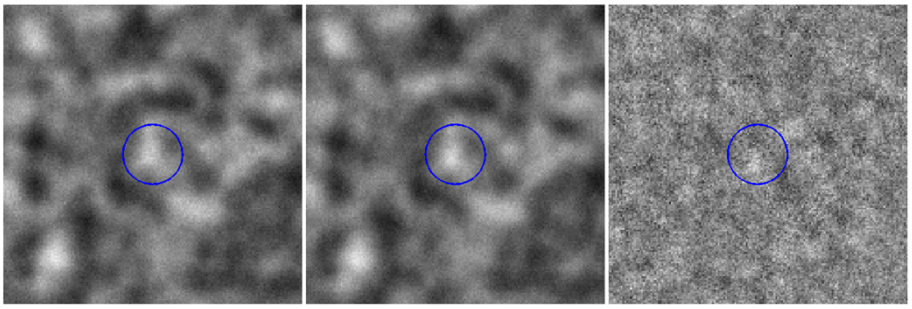

FIG. S5 From left to right are zoomed-in view of images taken are 240 s, 244.5 s, and the difference between the two images. The blue circle represents the characteristic length scale of the system.

S6. Sample intermediate scattering functions extracted from DDM measurements

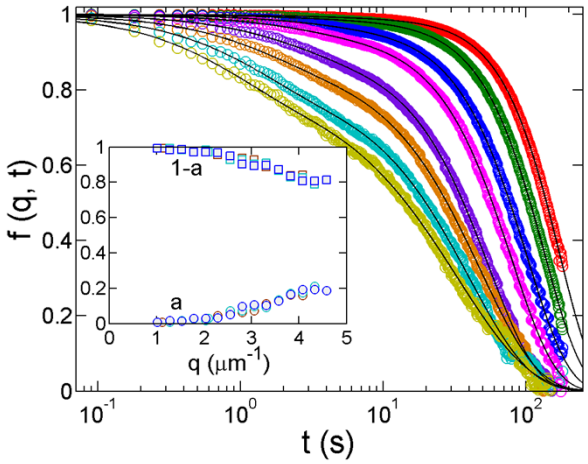

FIG. S6. Intermediate scattering functions, f(q,t), from DDM corresponding to the same data shown in Fig. 4b. Inset shows the fitting parameter a and corresponding 1-a at aging time of 4 (blue), 7 (cyan) and 10 minutes (brown), which becomes vanishingly small and approaches to 1 as q→0.

S7. Skewness of the distribution of intensity fluctuation, $\Delta\bar{I}^2$, probed by DDM

We extended the range of calculation on skewness shown in the inset of Fig. 5b, which decreases systematically with lag times until the data becomes too noisy.

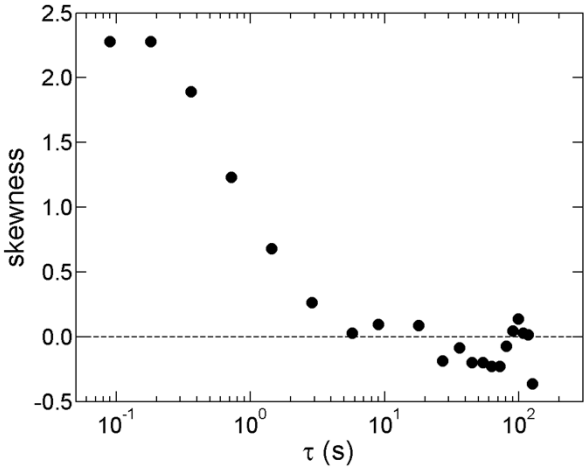

FIG. S7. Skewness of the distribution of intensity fluctuation, $\Delta\bar{I}^2$, probed at $q = q_{max}(t_{age})$ over an extended range of lag times.

S8. Effect of trajectory sampling on tracking of phase separated domains

Figure 6b shows that, when the entire ensemble of traceable domains is considered, the long-time MSD asymptotes to a scaling of $\langle \Delta r^2 \rangle \sim t^{1.35}$, which is potentially unexpected given the DDM result of $\beta = 2$ as $q \to 0$. It was hypothesized that the reason for discrepancy is an inability to track the dense domains for time periods such that the MSD exceeds that required to sufficiently sample the $q \to 0$ limit. To test this hypothesis, Figure S8 shows the corresponding average MSD considering only domains whose trajectories possess an end-to-end squared distance larger than ~20 μm^2, which represent the longest available trajectories, but are still smaller than the arrested value of $L_c^2 \sim 140$ μm^2. As evident in the figure, when only the trajectories sampling the largest space are considered, the MSD instead asymptotes to $\langle \Delta r^2 \rangle \sim t^{1.79}$, which is significantly closer to the expected scaling of t^2. We therefore conclude that the apparent discrepancy between the long-time MSD behavior of domain tracking measurements and the $q \to 0$ behavior of DDM measurements is indeed due to an inability to track domains for significantly long times before they coalesce.

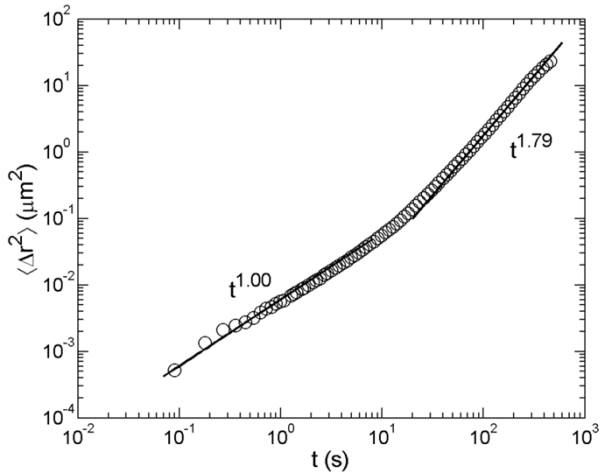

FIG. S8. MSD of fast-moving domains, i.e., those whose squared end-to-end distance are larger than ~20 μm^2.

S9. Two-point correlation function of domain motion

To examine the spatial correlation of coarsening domains, we calculate in Fig. S9 a two-point velocity-velocity correlation function,

$$C_{\vec{u}\vec{u}}(\Delta r, \Delta t) = \frac{< \vec{u}_i \cdot \vec{u}_j >}{< u^2 >}.$$

Here, $\vec{u}_i = \vec{r}_i(t + \Delta t) - \vec{r}_i(t)$ and $\vec{u}_j = \vec{r}_j(t + \Delta t) - \vec{r}_j(t)$ are the displacements of domain i and j, respectively. $\langle u^2 \rangle$ is the mean squared displacement and Δr is the distance between domains. The correlation function is fit to an exponential to extract a correlation length scale, which is shown in the inset of the right panel of Fig. S9. The characteristic length measured is smaller than Lc. This might due to the fact that the coarsening of domains is complex, which can happen in several different scenarios, such as domains (1) moving randomly due to thermal motion (no correlation) (2) moving towards (compression mode) or away from (expansion mode) each other (negative correlation) due to coalescence (3) moving in the same direction (translational mode) (positive correlation) possibly due to stress relaxation. The two point correlation function is an ensemble-average of all these possibilities, which might have smeared out the possible correlation. This suggests that correlated motion observed here is different from a supercooled liquid or glass and new devised metrics are required to properly capture the spatial correlation of motion of domains.

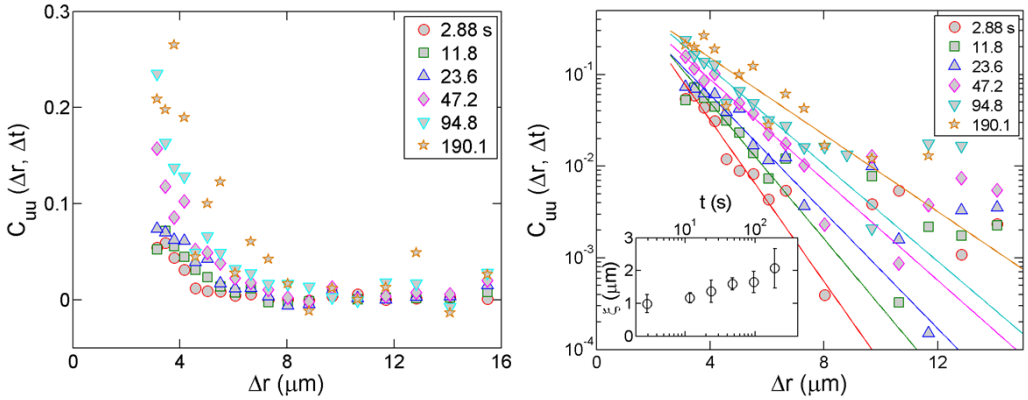

FIG. S9. Velocity-velocity correlation function of moving domains at different lag times. Results are shown in both a linear (left) and semi-logarithmic (right) plot. Solid lines are exponential fits to the data. Inset shows the corresponding characteristic length scales extracted from the fits.

Video S1 (available online): Raw video of the nanoemulsion sample undergoing coarsening used for the analysis in this work. The frame rate has been increased by a factor of 600 in order to enhance motion. Unidirectional thermal drift is apparent in the raw video. This drift is easily quantified using standard methods (see ref. [44] in main article), and is removed before performing any further analysis.

Video S2 (available online): Video showing time evolution of the best fit correlation coefficient map obtained by TAM analysis of the raw video in Video S1. Overlaid on top of the images are the trajectories of domains tracked over time. Cyan points indicated the beginning of each trajectory, and red points indicate its position in the current frame. The trajectory is colored green for the last frame in which the trajectory is traceable, in order to emphasize the disappearance of domains due to coalescence.

Supplementary References

[1] Cipelletti L, Manley S, Ball RC, Weitz DA. Universal aging features in the restructuring of fractal colloidal gels. *Physical Review Letters* **84**, 2275-2278 (2000).

[2] Duri A, Cipelletti L. Length scale dependence of dynamical heterogeneity in a colloidal fractal gel. *Europhysics Letters (EPL)* **76**, 972-978 (2006).

[3] Fluerasu A, Moussaid A, Madsen A, Schofield A. Slow dynamics and aging in colloidal gels studied by x-ray photon correlation spectroscopy. *Phys. Rev. E* 76, 010401 (2007).

[4] Guo H, Ramakrishnan S, Harden JL, Leheny RL. Gel formation and aging in weakly attractive nanocolloid suspensions at intermediate concentrations. *J. Chem. Phys*. 135, 154903 (2011).

[5] Madsen A, Leheny RL, Guo H, Sprung M, Czakkel O. Beyond simple exponential correlation functions and equilibrium dynamics in x-ray photon correlation spectroscopy. *New Journal of Physics* **12**, 055001 (2010).

[6] Chung B*, et al.* Microscopic Dynamics of Recovery in Sheared Depletion Gels. *Physical Review Letters* **96**, 228301 (2006).

[7] Manley S*, et al.* Glasslike Arrest in Spinodal Decomposition as a Route to Colloidal Gelation. *Physical Review Letters* **95**, 238302 (2005).

[8] Conrad JC*, et al.* Arrested fluid-fluid phase separation in depletion systems: Implications of the characteristic length on gel formation and rheology. *Journal of Rheology* **54**, 421 (2010).

[9] Dibble C, Kogan M, Solomon M. Structure and dynamics of colloidal depletion gels: Coincidence of transitions and heterogeneity. *Physical Review E* **74**, 041403 (2006).

[10] Gao Y, Kilfoil M. Direct Imaging of Dynamical Heterogeneities near the Colloid-Gel Transition. *Physical Review Letters* **99**, 078301 (2007).

[11] Royall CP, Williams, Stephen R., Ohtsuka, Takehiro and Tanaka, Hajime Direct observation of a local structural mechanism for dynamic arrest. *Nature materials* **7**, 556-561 (2008).